Research Square

Preprints are preliminary reports that have not undergone peer review.
They should not be considered conclusive, used to inform clinical practice,
or referenced by the media as validated information.

A Relationship Between Baroclinic Tidal and Wave Horizontal Spectral Energy and Stratification on the Australian Continental Shelf

Robin Robertson

robin.robertson@xmu.edu.my

Xiamen University Malaysia

Research Article

Keywords:

Posted Date: July 31st, 2026

DOI: https://doi.org/10.21203/rs.3.rs-10377328/v1

License: This work is licensed under a Creative Commons Attribution 4.0 International License. Read Full License

Additional Declarations: No competing interests reported.

Abstract

In order to investigate the seasonal dependence of the baroclinic kinetic energy, temperature and velocity data from sixteen moorings off Australia were analyzed. The sites ranged in latitude from ~12°S to 38°S and each had time series at least 4 years in length. The time series for each site were divided into 10-day segments to provide upper ocean to bottom temperature differences and baroclinic kinetic energy values for each segment. These values were then used to develop general relationships between the upper ocean to bottom temperature difference and the horizontal internal wave energy for five different frequency bands: diurnal, semidiurnal, harmonic (3-10 cpd), high frequency ($\geq$10 cpd), and all frequencies (0.167-12 cpd). These relationships followed a power law, $E_H = E_{BT}\ B\ dT^A$ where E_H represents the horizontal baroclinic spectral energy, E_{BT} is the horizontal barotropic spectral energy, dT is the upper ocean to bottom temperature difference, and A and B are latitude dependent coefficients. However, investigation of 12 additional sites showed no relationship between the upper ocean to temperature difference and the baroclinic energy and the velocities were essentially barotropic. Relationships were present only if the upper ocean to bottom temperature difference exceeded 4°C and the water depth was at least 60 m. These relationships can be useful in predicting the horizontal baroclinic energy fields for these frequency ranges without deploying and maintaining expensive velocity observations. The relationships can also be used to estimate the horizontal baroclinic energy available for mixing in models.

Key Points

• Relationships were found between the temperature difference between the upper ocean and the bottom and the internal wave and tidal energy

• Relationships differed for different frequency ranges and was strongest for diurnal and semidiurnal tides and all frequencies combined

• There was a latitude dependence of the coefficients for many of the frequency bands, particularly the tidal frequency bands

Plain English Summary

Tides and waves not only occur at the surface, but also between density layers within the ocean. These internal tides are important since they provide the energy for mixing of the different density layers of the ocean. Measuring the energy associated with these internal tides and waves in the field is much more expensive than measuring temperatures at two different depths. A relationship between the upper ocean and bottom temperature difference and the horizontal internal wave and tidal energy was developed. This relationship enables an estimate of the internal tidal and wave energy available for mixing in water depths ranging from 60-200 m without deploying expensive current meters, which can be used for both observations and models.

1 Introduction

Mixing is one of the key issues in ocean dynamics that is still not well defined, mostly due to the wide range of processes involved and their wide range of spatial and temporal scales. Internal tides and waves are big contributors to ocean mixing, both at the surface and in the deep ocean, particularly below the wave base. In shallow water, tidal mixing often results in a tidal front with well-mixed water on one side of the front and a stratified water column on the other.

Müller et al. (2014) note that a parameterization of the baroclinic tides is needed for the models to improve their handling of mixing. The present ocean models tend to overmix vertically (i. e. ROMS, Robertson and Dong, 2019). A new parameterization should be developed based on observations. However, measuring mixing and even the energy associated with the internal tides and waves is expensive, requiring the deployment and maintenance of current meters. If a relationship could be found to relate the temperature difference between the upper ocean, ~ 20 m depth, and the bottom it could provide estimates of the internal wave energy. Nash et al. (2012) postulate that it may not be possible to predict the coastal internal tides and he may be right that an exact prediction may be impossible. However, it might be possible to develop a parameterization of the locally generated

horizontal baroclinic kinetic energy that puts a range on the amount of horizontal baroclinic energy available for mixing based on the stratification and the barotropic tide.

Internal tides and waves vary with the stratification, which varies with the season. Many studies have been made of the seasonal dependence of the tides, using models (Cummins et al., 2000; Kang et al., 2002; Gerkema et al., 2012; Müller et al., 2012, Müller et al., 2014; Gräwe et al., 2014; Liu et al., 2019), observations (Holloway, 1988; Cottier et al., 2004; Eich et al., 2004, Katsumata et al., 2010; Georgas et al., 2012; Guo et al. 2012; Jeon et al., 2014; Devlin et al., 2017), or both models and observations (Yan et al., 2020; Subesh et al., 2025). Many of these studies investigated the seasonal variation of the barotropic tide, which varied dependent on the stratification. Studies based on satellite data are only able to evaluate the M_2 tide. These studies usually tied the seasonal barotropic variability to seasonal stratification associated wih changes in river flow or cyclone events (Kang et al., 2002; Müller et al., 2012). A few of the observational studies investigated the seasonality of the baroclinic tides (Holloway, 1988; Cottier et al., 2004; Katsumata et al., 2010). However, Yan et al. (2020) was the only one that investigated diurnal, semidiurnal, and several harmonic frequencies. These studies consistently found that the baroclinic tides and waves were stronger in the summer when the stratification was stronger. A link between the mean value and the amplitude of the baroclinic variations was found by Katsumata et al. (2010), but they did not link it with the stratification. None of these studies used time series over 2 years long and occasionally, utilized only a few select months in different seasons. This study only uses time series of at least 4 years duration, focusses on the temperature difference rather than the seasonality, and investigates the frequency dependence of the energy for the diurnal, semidiurnal, harmonic, and high frequency bands. The importance of separating the energy by frequency bands lies in identifying the energy transfers from the diurnal to the semidiurnal, semidiurnal to the harmonics, and harmonics to the high frequency, providing the energy for dissipation, in addition to looking at the overall energy.

Besides the seasonality, factors other than the stratification that can affect the baroclinic tides and internal waves are: critical latitudes, currents, eddies, fronts, wind, cyclones, storms, the evaporation/precipitation difference, water depth, the distance from the internal tide/wave generator, such as the continental shelf/slope break, and the topographic orientation. The diurnal tidal critical latitudes occur at 27.6^{o}S and 30°S for O_1 and K_1, respectively (Fig. 1). Diurnal tides are resonant at these latitudes, enabling an increase in energy transfers between frequencies through both harmonic and parametric subharmonic instabilities (psi) mechanisms. At the critical latitudes, tidal energy is trapped and spreads throughout the entire water column; whereas, away from the critical latitudes the tidal energy propagates away from the generating topography in beams focused at specific depths. Harmonic transfers were prominent in a modeling study of critical latitude effects over a seamount for the diurnal critical

latitudes (Robertson et al., 2017; Dong et al., 2019). Near the critical latitude, energy transfers were enhanced not only from the diurnal to the semidiurnal tides, but also to their harmonics and higher frequencies. The energy transfers to higher frequencies increased the turbulence and diapycnal mixing. The diapycnal mixing induced density-driven flows. This behavior occurred not only exactly at the critical latitudes, but also in a latitude band near the diurnal critical latitudes. Relative vorticity from current shear and eddies shifted the diurnal critical latitude away from their exact latitudes, sometimes by 1-2° (Dong et al., 2019). Additionally, a critical latitude like response occurred at 18°S, which was found to be dependent on the size of the seamount. So, topographic features can induce resonance at different latitudes and increase the energy transfers, turbulence, and mixing, similar to what occurs at the critical latitude. Some of the other factors, such as cyclones, storms, fronts, wind, and the evaporation-precipitation difference affect the stratification, the first four primarily through intensive mixing. Others, such as the topographic orientation affect the distribution of the horizontal velocities between the East-West and North-South components and can induce focusing effects (Eich et al, 2004). And others, such as the water depth and the distance from the internal tide/wave generators may be linked to each other.

In the pursuit of determining the seasonal dependence of the internal tidal and wave energy in mooring data off Australia, it was found that the upper ocean to bottom temperature difference provided a better estimate of the internal wave energy than the seasons. Of course, this temperature difference was primarily seasonal. A power relationship was found not only for the total baroclinic energy, but also for four additional frequency bands: diurnal (1 cpd), semidiurnal (2 cpd), harmonics (3–10 cpd), and high frequencies (> 10 cpd). Furthermore, some of the coefficients showed a latitude dependence and a relation for the latitude dependence for these coefficients was determined. The mooring data used for this analysis is described in Section 2 with the

analysis methods and relationship development in Section 3. The final relationships are given in Section 4 with the coefficients, their latitude dependence, and performance. Section 5 summarizes the study and gives ideas for future work.

2 Data

Temperature and velocity time series data from 66 moorings from the Integrated Marine Observing System (IMOS) were downloaded from the Australian Ocean Data Network (AODN; https://portal.aodn.org.au/) (Table S1 and yellow and magenta stars in Fig. 1). Of the time series from 66 mooring sites, 28 sites had both temperature data at 2 or more depths and simultaneous velocity data in time series that lasted 5 or more years. These 28 sites were selected for this study (Table 1). Most of these sites were located off the east coast of Australia (Fig. 1).

Before analysis, the data from different mooring deployments for each site was combined and reorganized so the time series for temperatures and velocities were at certain depths. At some sites the instrument deployment depths changed, so effort was made to have the depth of the time series with the least variation. An example of the reorganized data for the ORS065 temperature data is shown in Supplemental Figure S1 and the velocity data in Supplemental Figure S2. As part of the reorganization, a 3 point running mean was performed on the hourly data and spikes exceeding 3 standard deviations of the mean were removed as bad data. Most of the time series gaps, as seen in Supplemental Figures S1 and S2, are associated with maintenance of the moorings.

3 Methods

2.1 Spectral Analysis

Spectral analysis was performed on sections of the time series. Sections of length 5, 7.5, 10, 15, and 30 days with a 50% overlap were investigated. Due to monthly servicing of many of the moorings, the 15- and 30-day sections provided too few points. The 5- and 7.5-day sections lengths were chosen due to the typical storm frequency of 7 days, but their estimates were noisy, primarily due to the storms. The 10-day sections appeared to be the most representative of the general internal wave climate and the best choice for section length due to both the number of points and the lower noise.

Spectral analysis was performed on both the East-West and North-South velocities for 10-day sections with a 50% overlap over the length of the time series. The spectra from all the depths for that section were then averaged to provide an averaged spectrum for that section. The averaged spectrum for the section was integrated over 5 frequency bands: 1) total: all frequencies, 2) diurnal: frequencies between 0.5 and 1.5 cpd, 3) semidiurnal: frequencies between 1.5 and 2.5 cpd; 4) harmonics: or overtides frequencies between 3 and 10 cpd, and, 4) high frequencies: frequencies from 10 to 12 cpd (Fig. 2). The resultant spectra were

Table 1

Information on the 16 sites for which relationships between the upper ocean to bottom temperature difference and the horizontal baroclinic spectral energy were found, including, the location, the location code, the latitude and longitude, the water depth, the number of temperature and velocity files, the start date, the number of years, and the depths used for the temperature difference.

Site Code	Site Name	Latitude	Longitude	Water Depth (m)	No. of T Files	No. of V Files	Start Date	No. of Years	Temperature Depths (m)	Unstratified Criteria (°C)
ITFFTB	Indonesian Throughflow (ITF): Flat Tops Bank	12° 17.40' S	128° 28.63'E	103	85	17	26 Jun 2010	9+	25 100	1.5
ITFJBG	ITF: Joseph Bonaparte Gulf	13° 36.51' S	128° 58.00'E	59	59	18	25 Jun 2010	9+	23 55	0.5
GBRPPS	GBR: Palm Passage	18° 18.52' S	147° 9.93'E	60	184	33	28 Oct 2007	16+	22 60	1.0
GBRMYR	GBR: Myrmidon Reef	18° 13.17' S	147° 20.74'E	200	285	31	30 Oct 2007	16+	42 102	1.5
TAN100	Ningaloo	21° 51.00' S	113° 54.41'E	112	263	35	2 Aug 2010	14+	19 102	0.5
GBROTE	GBR: One Tree East	23° 28.99' S	152° 10.37'E	60	126	40	14 Sep 2007	16+	20 56	1.0
NRSNSI	North Stradbroke Island	27° 20.59' S	153° 33.72'E	60	28	35	4 Jun 2018	5+	21 58	0.5
CH070	Coffs Harbour 70m	30° 16.43' S	153° 17.94'E	70	567	62	12 Aug 2009	14+	28 60	1.0
CH100	Coffs Harbour 100m	30° 16.03' S	153° 23.68'E	100	887	58	12 Aug 2009	14+	24 93	1.5
WATR20	WA: Two Rocks 200m	31° 43.65' S	115° 2.37'E	200	216	23	15 Jul 2009	14+	30 155	1.0
ORSO65	Ocean Reference Station	33° 53.67' S	151° 18.88'E	65	2,910	185	7 Jun 2006	17+	19 60	1.0
SYD100	Sydney 100m	33° 56.56' S	151° 22.93'E	100	881	72	24 Jun 2008	16+	25 89	1.0
SYD140	Sydney 140m	33° 59.78' S	151° 26.21'E	140	1,117	71	24 Jun 2008	16+	32 134	1.5
PH100	Port Hacking 100m	34° 6.25' S	151° 11.20'E	100	929	55	28 Oct 2009	14+	33 89	1.5
BMP070	Bateman's Bay 70m	36° 11.43' S	150° 11.36' E	70	236	28	18 Nov 2014	9+	21 68	1.5
BMP120	Bateman's Bay 120m	36° 12.36' S	150° 18.87' E	119	597	29	25 Mar 2011	13+	28 116	1.5

normalized by both the number of days and the mean barotropic spectra for that site during the entire period. Normalizing by the barotropic spectral level reduced differences due to both different barotropic tidal magnitudes.

The average temperature difference from an upper ocean, usually ~ 20 m depth, and a continuous series near the bottom (Table 1) during the 10-day section was determined to provide the temperature difference for each section. Negative temperature differences were set as nans, as they represent internal wave breaking or overturning.

2.3 Relationship Development

The original goal was to investigate the seasonal dependence of the internal tidal and wave energy. Using ORS065 as an example, there is a clear seasonal dependence of the total, diurnal, and semidiurnal energies (Fig. 3). Investigation of the relationship of the temperature difference showed a clearer relationship than the seasonal dependence (Fig. 4), although the temperature difference is primarily seasonal. The temperature difference dependence occurred for all five frequency bands (Fig. 5), although it was weakest for the high frequences. It should be noted that the diurnal signal contains other daily processes than the tides, such as the daily overturning circulation in the upper ocean, land/sea breezes, and possibly diel migration. Also, there is more energy in the harmonic frequencies than the semidiurnal frequencies due to the wider frequency range for the harmonic band (Fig. 2).

A regression was fitted to the spectral energy and the temperature differences for all five frequency bands. Coefficients were determined through least squares regression for each of the mooring sites for each frequency band for the East-West, North-South, and Combined East-West and North-South spectral energies. Different regression types were tried including a square root (magenta for East-West and cyan lines for North-South in Fig. 5) and a power relation (black lines for East-West and green for North-South in Fig. 5). The solid lines in Fig. 5 are means of the coefficients and not based on the individual coefficients for each site. The dashed lines in Fig. 5 are the 95% confidence limits for the regression with the mean coefficients. The confidence limits were determined to identify the range of the energy values. The coefficients for each site are given in Tables S2-S4 for the Combined East-West and North-South velocities, East-West velocities, and North-South velocities, respectively. Both regressions in Fig. 5 have similar slopes; however, the power regressions are lower than the square root regressions, with the exception of the diurnal band, which is essentially equivalent for temperature differences greater than 1°C. Although linear internal wave theory predicts a square root relationship between the stratification represented by the Brunt-Väisälä frequency and the internal wave energy, a better fit was found for the power regression. Non-linearities arise from friction, advection, and other processes not accounted for in linear internal wave theory. Furthermore, the power regression coefficients showed a latitude dependence reflecting diurnal tidal critical latitude effects.

4 Results and Discussion

Although analysis was performed separately for the East-West, North-South, and total or combined East-West and North-South velocities, the discussion will focus on the total velocities. Generally, there was more energy in the East-West velocities than the North-South velocities; however, this partition is dependent on the topography and the orientation of the nearby continental shelf/slope break, the typical generator of the local internal tides and waves. Using the total velocities reduces the topographic influence and enables more general relationships between the internal tidal and wave energy and the stratification to be developed. The East-West and North-South coefficients are still provided. Furthermore, the discussion will focus on the mean; however, coefficients for both the lower and upper 95% confidence levels will be provided for those who require the range of values. The conversion of horizontal spectral energy into horizontal kinetic energy follows $KE_H = 0.5\ \rho < u'^2(z) + v'^2(z)>)>$, where KE_H is the horizontal kinetic energy, ρ is the density, u' and v' are the East-West and North-South baroclinic anomaly velocities, and < > indicates averaging, both over the 10-day period and the water column.

The power regression equation was $E_H = E_{BT}\ B\ dT^A$ where E_H represents the horizontal baroclinic spectral energy, E_{BT} is the horizontal barotropic spectral energy, dT is the upper ocean to bottom temperature difference, and A and B are coefficients. The spectral energy represents the horizontal kinetic energy for the frequency bands, although with a different magnitude dependent on the barotropic horizontal spectral level, the density, and a factor of 0.5. Since salinity was not present to determine density for many of the time series, no attempt was made to convert the spectral energy into kinetic energy.

However, due to the normalization by the barotropic energy, the barotropic spectral energy is needed to recover the baroclinic energy. For these sites, this could be provided by current meters. However, if there is no velocity record to provide the barotropic energy, an estimate of the barotropic tidal energy needs to be made. Since tides are the source of most of the energy, an estimate was made from the TPXO10v2a tidal velocities (Egbert and Erofeeva, 2002). The barotropic spectral energy was found to follow $E_{BT} = 5.6\ \Sigma(au^2 + av^2)$, where the summation is over all 25 tidal constituents and au and av are the East-West and North-South amplitudes, respectively, for each constituent. This relationship does not work well if the depth used by TPXO10v2a is significantly (> 40%) different than the depth of the site or for ITFFTB or ITFJBG, which are in exceptionally strong tidal region. TPXO10v2a gives barotropic tidal velocities exceeding 5.0 and 8.0 m/s for these two sites, which are extremely large.

Site specific coefficients will reproduce the baroclinic kinetic energy most accurately, but a generalized relationship is more useful for estimates of horizontal baroclinic kinetic energy. The means of the coefficients for each frequency band and velocity are given in Table 2 and the mean regressions and values are shown as blue lines in Figs. 6–7 and Supplemental Figures S3-S10. The values in Figs. 6 and 7 are integrated over the entire frequency range. Site specific A and B coefficients and their 95% confidence limits are shown in Fig. 8 in red for the East-West (red), North-South (blue), and total (black) velocities. It should be noted that the ITFFTB and ITFJBG A coefficients are slightly negative for the semidiurnal band (Fig. 8), indicating an exponential relationship instead of a power relationship. As mentioned before these two sites are in an extremely strong tidal regime on the northern Australian continental shelf. They are also in the neighborhood of the Indonesian Throughflow and have potential to be influenced by internal tides and waves generated in the Timor Sea. This is a very active region of internal tide and wave generation (Robertson and Ffield, 2008; Robertson, 2010, Robertson, 2011)

The relationship between the stratification represented by the temperature difference and the horizontal spectral energy for sites equatorward of 27°S, the O_1 critical latitude, are shown in Fig. 6 and those within and poleward of the diurnal critical latitude band in Fig. 7. The regression lines in Figs. 6 and 7 for the mean value are shown in blue with the 95% confidence limits indicated by blue dashed lines. These regression lines are based on the mean coefficient values for all sites and not the individual coefficients for the sites. The regression with the mean values underestimates the spectral levels for most of the sites equatorward of the diurnal critical latitude range, with exceptions of TAN100 and GBRPPS (Fig. 6). It is possible that there is an enhancement of the energy at these two sites due to topographic resonance, since they are in the neighborhood of many reefs of varying topographic size. The performance of the mean regression is better for sites in and poleward of the diurnal critical latitude range, with the exception of NRSNSI and WATR20.

The individual coefficients A and B are for each site are shown in Fig. 8 and given in Supplemental Tables S2-S4 for the combined East-West and North-South velocities (black), the East-West velocities (red), and the North-South velocities (blue), respectively. Note that in Fig. 8 and Table 1, there are 3 groupings of sites, which are close together in latitude, but in different water depths. In these pairs, the deeper site(s) is(are) usually at 100 m or deeper and the shallower site at 60–70 m. The deeper sites had higher spectral densities by a factor of 2-2.5. Furthermore, the East-West coefficients were typically smaller than the North-South velocities. Note that the A coefficient is the exponent and an A coefficient of 0.5 is equivalent to a square root, which is the relation according to linear internal wave theory. Generally, the A coefficient was less than 0.5, indicating frictional and other non-linear effects. The B coefficient controls the magnitude of the kinetic energy. Looking at the A coefficient for the diurnal band (Fig. 8a), there are several high points associated with GBRPPS, GBRMYR, GBROTE, and WATR20. There are some differences with these sites. GBRPPS, GBRMYR, and GBROTE are located in the Great Barrier Reef, which has both a wider continental shelf and very complicated topography due to the many reefs. GBRMYR and WATR20 are located in water depths of 200 m, and are ,much deeper than the other sites. WATR20 was also located at the end of a canyon, so specific topographic effects come into play. The deep temperature at WATR20 was at 155 m, 45 m above the bottom, whereas with the exception of GBRMYR, at the other sites, the deep temperature was typically within 5 m of the bottom. Additionally, the WATR20 site has an extremely high B coefficient (Fig. 8f)

Relationships were only found for 16 of the 28 sites. If the temperature difference was less than 4°C or the water depth was shallower than 60 m or greater than 200 m, there was no clear relationship between the upper ocean to bottom temperature difference and the baroclinic spectral energy (Fig. 9). Note that Fig. 9 contains both the East-West) (red) and North-South (blue) velocities, resulting in two groupings of velocities. Reasons that there was no relationship are given for the 12 sites in

Supplemental Table S5. Although there was no relationship, there was a range of energies for those sites. There was also no relationship between the barotropic kinetic energy and the temperature difference (Supplemental Figure S11), although again, there was a general range of values, which differed for the East-West and North-South velocities (Supplemental Figure S11). Although relationships between stratification and the barotropic kinetic energy have been found, typically they have been locations where the salinity changes significantly during the year due to variations in river runoff or monsoonal rains. Australia is a dry continent and although rainfall changes significantly during storm and cyclone events, river runoff is generally low.

Table 2
Mean A and B coefficients for the five frequency bands for the East-West, North-South, and Combined velocities. The mean barotropic tidal energy is given for each velocity and frequency band.

Combined East-West and North-South Velocities					
Frequency Band	A for All	B			Mean Barotropic Spectral Density ($m^2 s^{-2}$)
		Mean	Low 95% Confidence	High 95% Confidence	
All Frequencies	0.326	0.022	0.009	0.108	41,275
Diurnal (1 cpd)	0.323	0.992	0.412	4.81	120
Semidiurnal (2 cpd)	0.366	0.531	0.221	2.57	41
Harmonics (3–10 cpd)	0.281	0.847	0.352	4.11	51
High Frequency (≥ 10 cpd)	0.254	0.779	0.323	3.77	10
East-West Velocities					
Frequency Band	A for All	B			Mean Barotropic Spectral Density ($m^2 s^{-2}$)
		Mean	Low 95% Confidence	High 95% Confidence	
All Frequencies	0.286	0.042	0.017	0.202	739
Diurnal (1 cpd)	0.326	1.45	0.602	7.03	34
Semidiurnal (2 cpd)	0.374	0.840	0.349	4.07	20
Harmonics (3–10 cpd)	0.255	1.48	0.614	7.17	15
High Frequency (≥ 10 cpd)	0.211	1.45	0.601	7.02	3
North-South Velocities					
Frequency Band	A for All	B			Mean Barotropic Spectral Density ($m^2 s^{-2}$)
		Mean	Low 95% Confidence	High 95% Confidence	
All Frequencies	0.336	0.019	0.008	0.092	33,877
Diurnal (1 cpd)	0.309	0.823	0.342	3.99	86
Semidiurnal (2 cpd)	0.346	0.440	0.183	2.13	21
Harmonics (3–10 cpd)	0.280	0.686	0.285	3.33	37
High Frequency (≥ 10 cpd)	0.264	0.630	0.261	3.05	8

Both the A and B coefficients varied per site (Fig. 8). For some frequencies, the coefficients were roughly constant or had no clear pattern. However, a latitude dependence was evident for some frequencies, primarily for the B coefficient, which determined the magnitude. The semidiurnal coefficient behavior often changed with relation to the diurnal critical latitudes (Fig. 8b and 8g). With the exception of the Great Barrier Reef stations and WATR20, both the A and B coefficients for the semidiurnal band increased within and poleward of the diurnal critical latitude range (Fig. 8b and 8g). The A coefficient, representing the exponent, for the diurnal band generally increased with latitude from the low latitudes to the critical latitude range, with the exception of the Great Barrier Reef stations. The B coefficient for the harmonic and high frequency bands generally decreased with increasing latitude poleward of 15°S. For the overall spectral density for all frequencies, there was no consistent pattern for the A coefficient, indicating exchanges between frequencies, cancelling the opposing trends of the frequency bands (Fig. 8e). For the B coefficient for all frequencies, there was a general decrease with increasing latitude, with the exception of ITFFTB (Fig. 8j). Past internal wave studies by the author showed transfers of energy from the diurnal frequencies to the semidiurnal frequencies near the diurnal critical latitudes (Robertson et al.,2017; Dong et al., 2019). Thus, energy lost from the diurnal frequencies goes to the semidiurnal frequencies and harmonics and this is reflected in the coefficients, particularly the magnitude coefficient, B. Some of the poor performance may be due to the presence of the East Australian Current (EAC) at the sites along the east coast. Currents interact with the baroclinic tides modulating their size.

To investigate the latitude dependence of the coefficients, a linear regression was performed. The general formulas were $A = C_1 |\psi| + C_2$ and $B = C_3 |\psi| + C_4$, where ψ is the latitude and the C's are coefficients. The absolute value of the latitude is used here, so it can be applicable in either hemisphere, although only data from the Southern Hemisphere was used for its derivation. However, the physics should be the same in both hemispheres. The C coefficients are given in Table 3 and shown for the different sites in Fig. 10 for the East-West (red), the North-South (blue), and combined (black). The latitude dependent coefficient regressions are shown in Figs. 6, 7, and S3-10 as red lines with their 95% confidence limits as dashed red lines. The latitude dependent coefficients performed better than the mean coefficients, particularly for the semidiurnal frequencies with lower rms differences (Table 4) and a better match with the observations for most sites (Figs. 6,7, and S3-10).

The best performance is with site specific coefficients; however, that is not practical since time series of four or more years do not exist for many sites. Latitude dependent coefficients give the next best performance, followed by using mean coefficients over all sites. However, the mean coefficients here are biased towards the diurnal critical latitude range since more of the sites are located there, reducing its applicability. A simpler method may yield equivalent performance to using a mean value for the coefficients. Investigating the time since the water column was unstratified ($dT < 1.5^{o}C$), typically, there was an increase in baroclinic kinetic energy during the first 15 days, after which it remained at a relatively constant level. It would be much simpler to implement such a parameterization in a model to evaluate the time since the upper ocean to bottom temperature difference was $\geq 1.5^{o}C$, then use a latitude dependent level. For

Table 3

Coefficients C_1, C_2, C_3, and C_4 to determine the latitude dependent coefficients A and B for the East-West, North-South, and Combined East-West and North-South velocities. Only C_4 varies for the mean, and low and high 95% confidence levels.

Combined East-West and North-South Velocities						
Frequency Band	C_1	C_2	C_3	C_4	C_4	C_4
	All	All	All	Mean	Low 95%	High 95%
All Frequencies	0.0070	0.135	-0.048	-0.358	-0.736	0.328
Diurnal (1 cpd)	0.0067	0.139	-0.008	0.215	-0.167	0.901
Semidiurnal (2 cpd)	0.0204	-0.191	-0.0007	-0.255	-0.637	0.430
Harmonics (3–10 cpd)	0.0063	0.110	-0.019	0.446	0.064	1.13
High Frequency (≥ 10 cpd)	0.0015	0.212	-0.030	0.715	0.334	1.40
East-West Velocities						
Frequency Band	C_1	C_2	C_3	C_4	C_4	C_4
	All	All	All	Mean	Low 95%	High 95%
All Frequencies	0.010	0.018	-0.023	-0.759	-1.14	-0.074
Diurnal (1 cpd)	0.011	0.024	0.022	0.102	-0.279	0.788
Semidiurnal (2 cpd)	0.028	-0.374	0.018	-0.577	-0.959	0.109
Harmonics (3–10 cpd)	0.011	-0.034	0.004	0.056	-0.326	0.742
High Frequency (≥ 10 cpd)	0.005	0.081	-0.004	0.259	-0.123	0.944
North-South Velocities						
Frequency Band	C_1	C_2	C_3	C_4	C_4	C_4
	All	All	All	Mean	Low 95%	High 95%
All Frequencies	0.007	0.156	-0.055	-0.224	-0.606	0.461
Diurnal (1 cpd)	0.006	0.156	-0.013	0.280	-0.102	0.966
Semidiurnal (2 cpd)	0.017	-0.117	-0.010	-0.097	-0.479	0.588
Harmonics (3–10 cpd)	0.004	0.179	-0.030	0.663	0.281	1.35
High Frequency (≥ 10 cpd)	0.0003	0.257	-0.042	0.937	0.555	1.62

Table 4
Mean total RMS differences between the observed values and the estimated values using the coefficients from all 16 sites for the mean and latitude dependent coefficients for the East-West, North-South, and Combined velocities.

Frequency Band	Combined East-West and North-South		East-West		North-South	
	Mean	Latitude Dependent	Mean	Latitude Dependent	Mean	Latitude Dependent
All Frequencies	$1.0x10^9$	$6.6x10^8$	$1.1x10^8$	$1.0x10^8$	$5.7x10^8$	$3.5x10^8$
Diurnal (1 cpd)	$3.0x10^7$	$1.9x10^7$	$6.5x10^6$	$4.0x10^6$	$9.3x10^6$	$7.0x10^6$
Semidiurnal (2 cpd)	$1.0x10^6$	$4.0x10^5$	$2.3x10^5$	$6.9x10^4$	$3.6x10^5$	$2.0x10^5$
Harmonics (3–10 cpd)	$2.2x10^7$	$1.7x10^7$	$2.1x10^6$	$1.5x10^6$	$1.4x10^7$	$1.2x10^7$
High Frequency (≥ 10 cpd)	$1.8x10^6$	$1.6x10^6$	$1.3x10^5$	$1.2x10^5$	$1.3x10^6$	$1.2x10^6$

the times that the temperature difference is < 1.5^{o}C, a linear estimate can be made dependent on the temperature difference, bringing it to that level. The final level would be latitude dependent and follow the latitude dependent coefficients for temperature differences greater than 4°C. The ramp up of the horizontal baroclinic kinetic energy during the first 15 days would also follow the latitude dependent coefficients ramping up from a temperature difference of 0.1-1.5^{o}C.

5 Conclusions

Temperature and velocity data from 28 mooring sites off Australia were analyzed for their upper ocean (~ 20 m) to bottom temperature differences and the horizontal baroclinic spectral energy for five frequency bands: diurnal (1 cpd), semidiurnal (2 cpd), harmonic (3–10 cpd), high frequencies (10–12 cpd), and all frequencies (0.167-12 cpd). The data was broken into 10-day segments in order to investigate the stratification dependence of the internal tidal and wave energy. For 16 of the 28 mooring sites a relationship existed between the upper ocean to bottom temperature difference and the baroclinic kinetic energy. Since salinity data was not available for many of the moorings, this temperature difference was used to represent the stratification, realizing the shortcoming of not using density. However, for 12 sites, there was no relationship. These 12 sites either had very small temperature differences, often only 1°C and always less than 4°C, or were in shallow water, less than 60 m deep, or deep water, greater than 200 m. Sixteen mooring sites showed a power relationship between the upper ocean to bottom temperature difference and the horizontal baroclinic kinetic energy as represented by the spectral density of the horizontal velocities following $E = E_{BT}\ B\ dT^A$. The coefficients A and B varied for the different frequency bands (Supplemental Tables S2-4). Furthermore, A had a latitude dependence for the diurnal and semidiurnal bands and B a latitude dependence for most frequency bands (Table 3). Coefficients were found to relate the coefficients to the latitude: $A = C_1\ |\psi| + C_2$ and $B = C_3\ |\psi| + C_4$, where ψ is the latitude. The best performance, defined as replicating the original values, occurred with site specific coefficients. However, reasonable performance was attained for a general relationship using mean values for the coefficients (Table 2). Performance improved and the rms differences reduced for the semidiurnal band when latitude dependent coefficients were used, reflecting critical latitude effects on the energy transfers between frequencies. It should be noted that these relationships are probably limited to sites on the continental shelf near the continental shelf-slope break and only represent local generation.

These relationships can be used to estimate the locally-generated baroclinic kinetic energy available for the five frequency ranges without deployment of expensive current meters. They could also be useful for tuning the sub-grid cell mixing parameterizations in models, particularly ones which do not include tides in their dynamics. Furthermore, it is possible that a simpler relationship could be found. Many of the sites increased for the first 7–15 days after they were unstratified and then reached a basic level or band once the temperature difference reached 1.5-2°C. A simpler formulation could be based on this behavior using the latitude dependent coefficients to set the basic level. In conclusion, these relationships might not be able to predict the coastal baroclinic tides as posed by Nash et al. (2012); however, they can make a step in that direction by providing a range of horizontal baroclinic

kinetic energy for different frequency ranges based on the barotropic tidal energy, as determined by the TOPEX10 tidal estimates. Thus, these relationships can provide a parameterization of the baroclinic tidal and wave mixing as desired by Müller (2012).

There are ways to improve these estimates. First, additional long-term, > 4 years, sites from other locations could be included to check if the relations hold there also and potentially to strengthen the relationships. The deeper sites had roughly 2-2.5 times the baroclinic kinetic energy of the shallower sites and more accurate coefficients could be found if water depth was accounted for. Unfortunately, the number of pairs of points at the same latitudes was insufficient to develop such a relation. Additionally, the relationships represent the average baroclinic kinetic energy per site and say nothing about the depth distribution of that energy. Depth-dependent relationships would be more useful, although they would probably be dependent on distance from the continental shelf/slope break. Furthermore, the barotropic spectral energy estimate has room for improvement. With sufficient data, the impacts of other factors than the stratification and latitude could be investigated, including currents, eddies, fronts, wind, the evaporation/precipitation difference, cyclones, storms, water depth, the distance from the internal tide/wave generator, such as the continental shelf/slope break, and the topographic orientation.

Declarations

Open Research

All the data used for this study were collected as part of the Integrated Marine Observing System (IMOS). They are available through the Australian Open Data Network (AODN) and can be found at the AODN portal https://portal.aodn.org.au/. The software used for analysis was performed using Matlab and is available from the author upon request.

Conflict of Interest Disclosure

The author declares there are no conflicts of interest for this manuscript.

Author Contribution

The lead author did all the research, analysis, writing and editing for this paper.

Acknowledgments

A majority of this research was performed when the lead author was retired and an Adjunct Professor with Xiamen University Malaysia. No funding has been provided for this research.

Data Availability

All the data used in this research is openly available on the Australian Open Data Network (AODN).

References

1. Cottier F, Inall M, Griffiths C (2004) Seasonal variations in internal wave energy in a Scottish sea loch. Ocean Dyn 54(3–4):340–347. https://doi.org/10.1007/s10236-003-0064-5
2. Cummins PF, Masson D, Foreman MGC (2000) Stratification and mean flow effects on diurnal tidal currents off Vancouver Island. J Phys Oceanogr 30(1):15–30. 10.1175/1520-0485(2000)030%3C0015:SAMFEO%3E2.0.CO;2
3. Devlin AT, Jay DA, Zaron ED, Talke SA, Pan J, Lin H (2017) Tidal variability related to sea level variability in the Pacific Ocean. J Geophys Research: Oceans 122(11):8445–8463. https://doi.org/10.1002/2017JC013165

4. Dong J, Robertson R, Dong C, Hartlipp PS, Zhou T, Shao Z, Lin W, Zhou M, Chen J (2019) impacts of mesoscale currents on the diurnal critical latitude dependence of internal tides: A numerical experiment based on Barcoo Seamount. J Geophysical= Research: Oceans 124(4):2452–2471. 10.1029/2018JC014413
5. Eich ML, Merrifield MA, Alford MH (2004) Structure and variability of semidiurnal internal tides in Mamala Bay, Hawaii. J Geophys Research: Oceans 109:C05010. 10.1029/2003JC002049
6. Egbert GD, Erofeeva EV (2002) Efficient inverse modeling of barotropic ocean tides. J Atmos Ocean Technol 19(2):183–204. 10.1175/1520-0426(2002)019%3C0183:EIMOBO%3E2.0.CO;2
7. Georgas N (2012) Large seasonal modulation of tides due to ice cover friction in a midlatitude estuary. J Phys Oceanogr 42(3):352–369. https://doi.org/10.1175/jpo-d-11-063.1
8. Gerkema T, Lan F-PA, Mass RM (2012) Internal tides in the Bay of Biscay; Conversion rates and seasonal effects. Deep-Sea Res Part II 51(25–26):2995–33008. 10.1016/j/dsr2.2004.09.012
9. Gräwe U, Burchard H, Müller M, Schuttelars HM (2014) Seasonal variability in M_2 and M_4 tidal constituents and its implications for the coastal residual sediment transport. Geophys Res Lett 41(15):5563–5570. https://doi.org/10.1002/2014GL060517
10. Guo P, Fang W, Liu C, Qiu F (2012) Seasonal characteristics of internal tides on the continental shelf in the northern South China Sea. J Geophys Research: Oceans 117(C4):C04023. https://doi.org/10.1029/2011jc007215
11. Holloway PE (1988) Climatology of internal tides at a shelf break location on the Australian North West Shelf. Mar Freshw Res 39:1–18. 10.1071/MF988001
12. Jeon C, Park J-H, Varlamov SM, Yoon J-H, Kim YH, Seo S (2014) Seasonal variation of semidiurnal internal tides in the East/Japan Sea. J Geophys Research: Oceans 119(5):2843–2859. https://doi.org/10.1002/2014JC009864
13. Kang SK, Foreman MGG, Lie H-J, Lee J-H, Cherniawsky J, Yum K-D (2002) Two-layer tidal modeling of the Yellow and East China Seas with application to seasonal variability of the M^2 tide. J Geophys Research: Oceans 107(C3):6–1. https://doi.org/10.1029/2001JC000838
14. Katsumata K, Wijffels SE, Steinberg CR, Brinkman R (2010) Variability of the semidiurnal internal tides observed on the Timor Shelf. J Geophys Research: Oceans 115(C10):C10008. https://doi.org/10.1029/2009jc006071
15. Liu K, Sun J, Guo C, Yang Y, Yu W, Wei Z (2019) Seasonal and spatial variations of the M_2 internal tide in the Yellow Sea. J Geophys Research: Oceans 124. https://doi.org/10.1029/2018JC014819
16. Müller M (2012) The influence of changing stratification conditions on barotropic tidal transport and its implications for seasonal and secular changes of tides. Cont Shelf Res 47(0):107–118. https://doi.org/10.1016/j.csr.2012.07.003
17. Müller M, Cherniawsky JY, Foreman MGG, von Storch J-S (2014) Seasonal variation of the M_2 tide. Ocean Dyn 64(2):159–177. https://doi.org/10.1007/s10236-013-0679-0
18. Nash JD, Shroyer EL, Kelly SM, Inall ME, Duda TF, Levine MD, Jones NL, Musgrave RC (2012) Are any coastal internal tides predictable? Oceanography 25(2):80–95. https://doi.org/10.5670/oceanog.2012.44
19. Robertson R (2011) Interactions between tides and other frequencies in the Indonesian Seas. Ocean Dyn 61:69–88. 10.1007/s10236-010-0343x
20. Robertson R (2010) Tidal Currents and mixing at the INSTANT mooring locations. Dyn Atmos Oceans 50:331–373. 10.1016/j.dynatmoce.2010.02.004
21. Robertson R, Dong CM (2019) An evaluation of the performance of vertical mixing parameterizations for tidal mixing in the Regional Ocean Modeling System (ROMS). Geoscience Lett 6(15). 10.1186/s40562-019-0146-y
22. Robertson R, Dong J, Hartlipp P (2017) Diurnal Critical Latitude and the Latitude Dependence of Internal Tides, Internal Waves and Mixing. J Geophys Research: Oceans 122(10):7838–7866. 10.1002/2016jc012591
23. Robertson R, Ffield A (2008) Baroclinic Tides in the Indonesian Seas: Tidal Fields and Comparisons to Observations. J Geophys Research: Oceans. 10.1029/2007JC004677
24. Subeesh MP, Song H, Addad Y, Scott JR, Marshall J, Al Shehhi MR (2025) Seasonality of internal tides in the Strait of Hormuz: Observations and modeling. J Geophys Research: Oceans 130:e2024JC021007. https://doi.org/10.1029/2024JC021007

25. Yan T, Qi Y, Jing Z, Cai S (2020) Seasonal and spatial features of barotropic and baroclinic tides in the northwestern South China Sea. *Journal of Geophysical Research: Oceans*, 125, e2018JC014860. https://doi.org/10.1029/2018JC014860

Figures

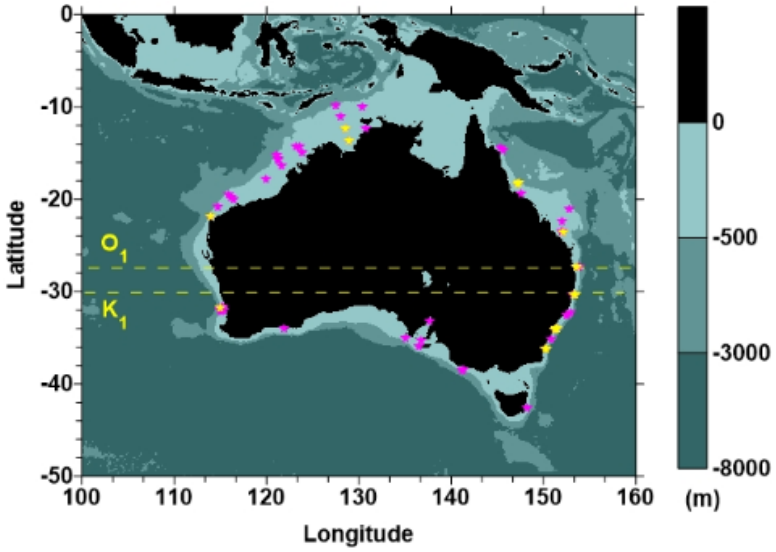

Figure 1

The bathymetry of the waters around Australia with the sites of the 66 moorings indicated by magenta stars. The 16 sites that were used are indicated by yellow stars. The K_1 and O_1 diurnal critical latitudes are indicated by dashed yellow lines.

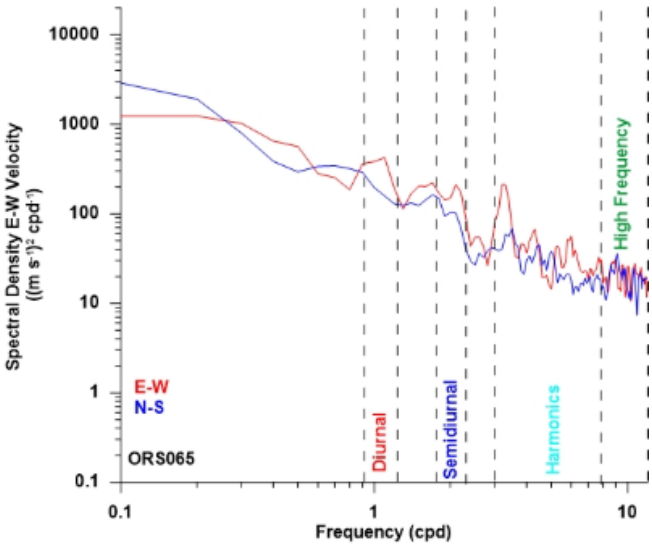

Figure 2

Baroclinic spectra from ORS065 using 10-day sections averaged over all depths for the East-West (red) and North-South (blue) velocities. The limits of the frequency bands used for integration are indicated with dashed lines and labeled.

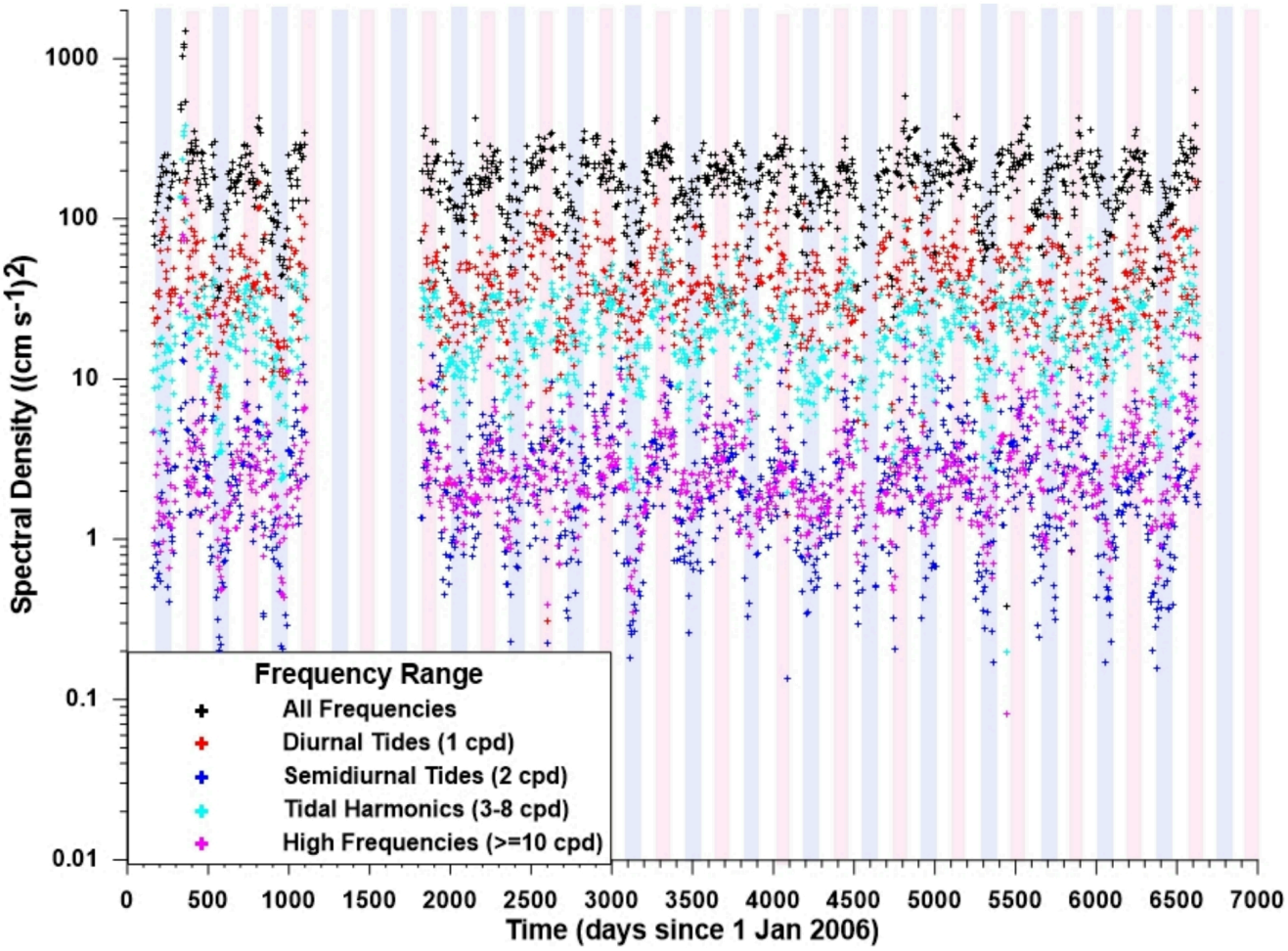

Figure 3

Time series of the baroclinic spectral density for five different frequency bands: all frequencies (black), diurnal (1 cpd) (red), semidiurnal (2 cpd) (blue), harmonics (3-10 cpd) (cyan), and high frequencies (> 10 cpd) (magenta). Summer and winter are represented by pink and light blue vertical bands, respectively.

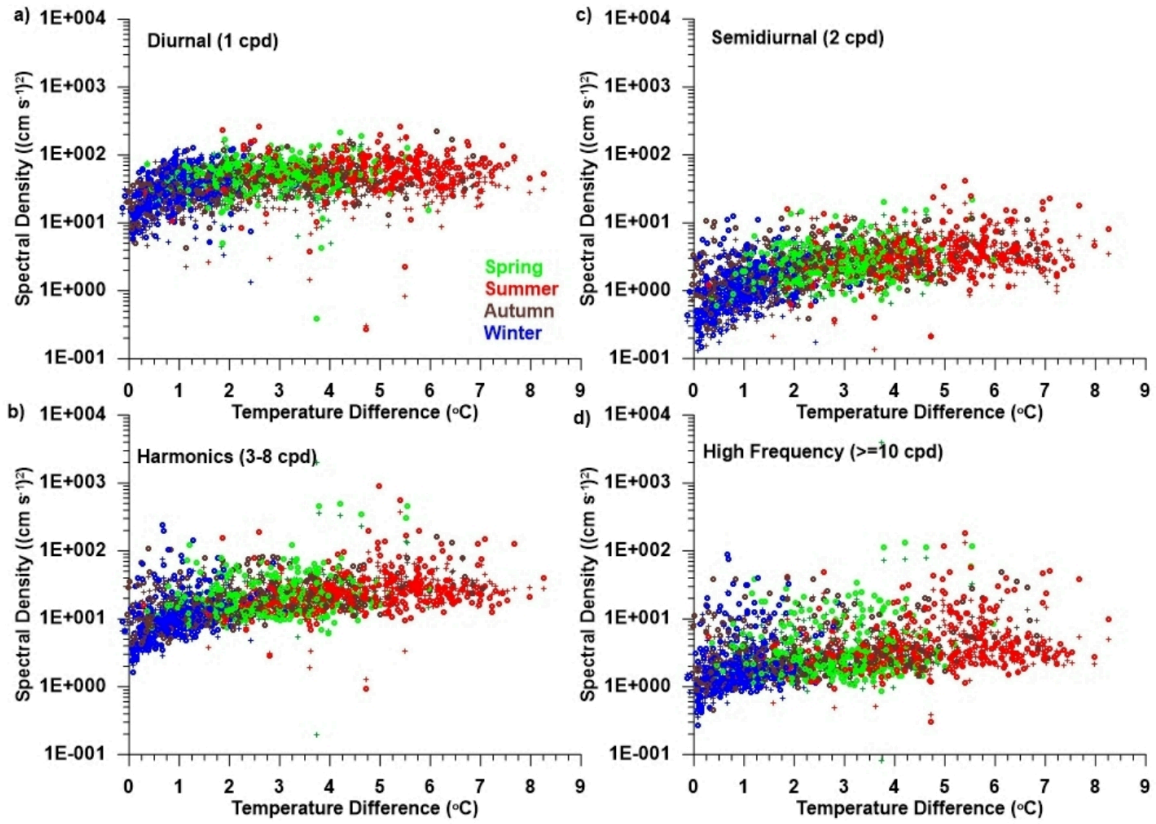

Figure 4

The baroclinic spectral density versus the upper ocean to bottom temperature difference for four frequency bands a) diurnal, b) harmonics (3-10 cpd), c) semidiurnal, and d) high frequency (>10 cpd) from the data at ORS065. The season is indicated by the color with summer as red, autumn as brown, winter as blue, and spring as green.

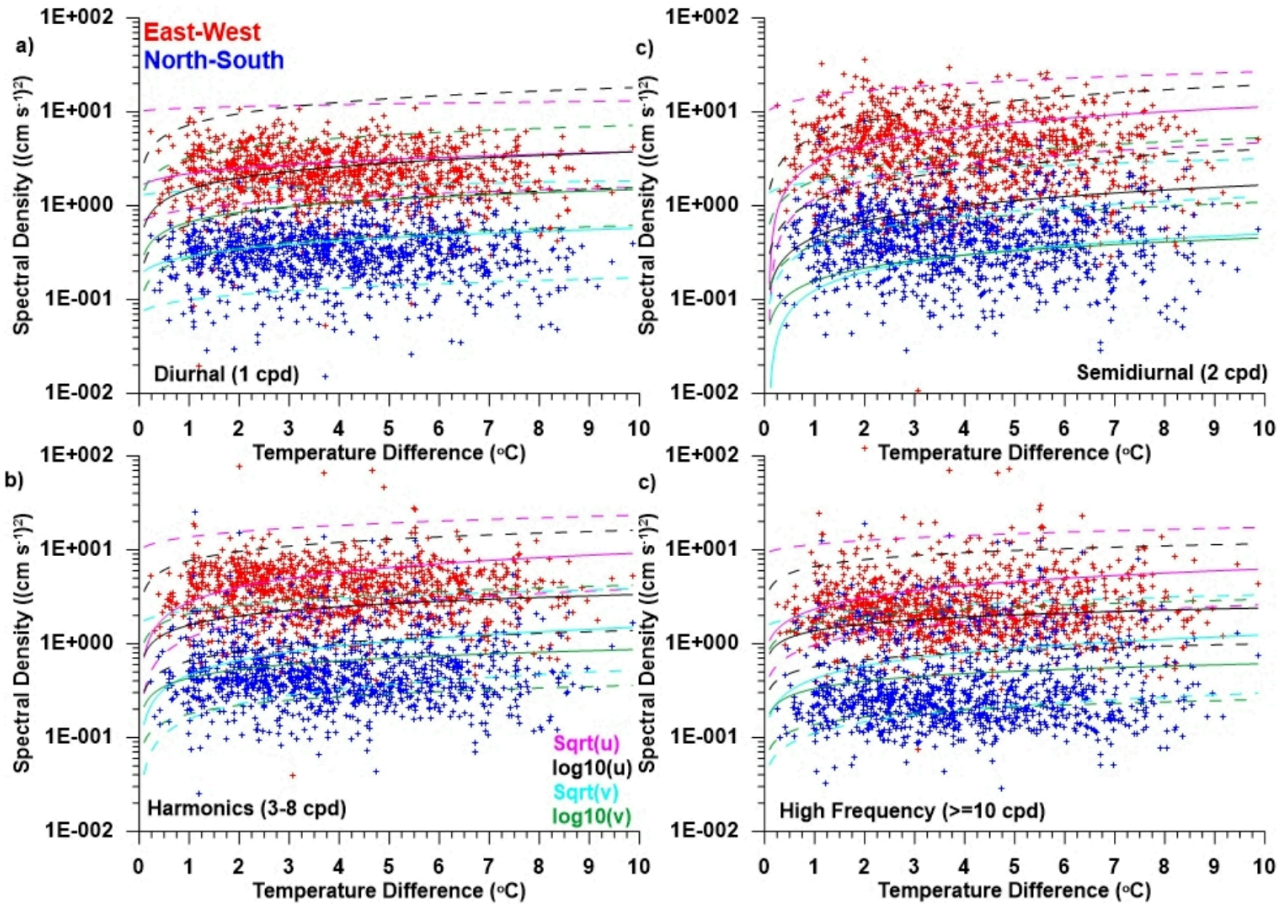

Figure 5

The baroclinic spectral density versus the upper ocean to bottom temperature difference from the data at ORS065 with the East-West velocity points as red and the North-South velocity points as blue for four frequency bands; a) diurnal, b) harmonics (3-10 cpd), c) semidiurnal, and d) high frequency (>10 cpd). Regression lines are shown for the square root for the East-West velocity in magenta and the North-South velocity in cyan. The power regression lines are indicated for the East-West velocity in black and the North-South velocity in green. The dashed lines indicate the 95% confidence limits. The regression lines in this figure are for the individual site and are not generalized for all sites.

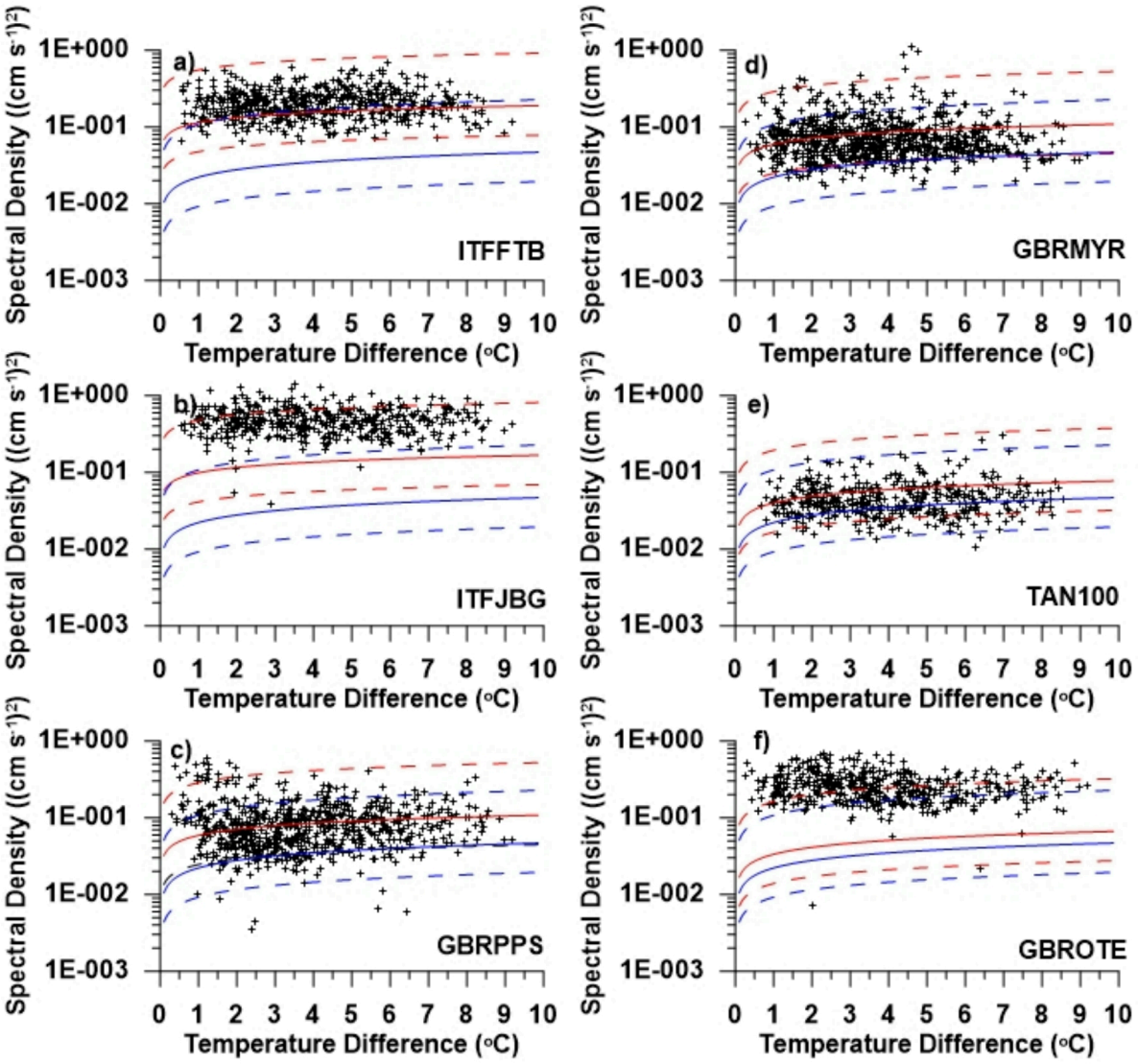

Figure 6

The baroclinic spectral density versus the upper ocean to bottom temperature difference for combined East-West and North-South velocities integrated over all spectral frequencies for sites equatorward of the diurnal tidal critical latitude range: a) NRSNSI, b) CH070, c) CH100, d) WATR020, e) ORS065, f) SYD100, g) SYD140, h) PH100, i) BMP070, and j) BMP120. The power regression lines are shown in blue for the mean coefficients and in red for the latitude dependent coefficients. The dashed lines indicate the 95% confidence limits. The regression lines in this figure used the generalized relations.

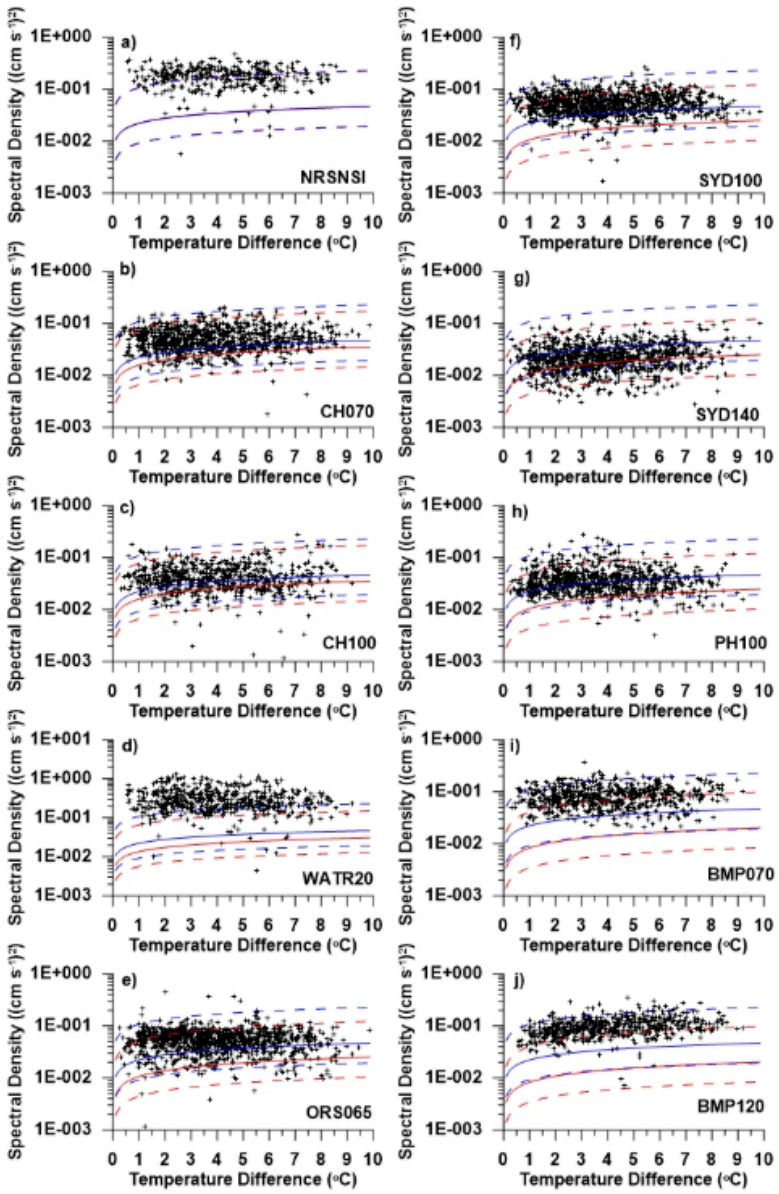

Figure 7

The baroclinic spectral density versus the upper ocean to bottom temperature difference for combined East-West and North-South velocities integrated over all spectral frequencies for sites in or poleward of the diurnal tidal critical latitude range: a) ITFFTB, b) ITFJBG, c) GBRPPS, d) GBRMYR, e) TAN100, and f) GBTOTE. The power regression lines are shown in blue for the mean coefficients and in red for the latitude dependent coefficients. The dashed lines indicate the 95% confidence limits. The regression lines in this figure used the generalized relations. Sites NRSNSI, CH070, and CH100 are in the diurnal tidal critical latitude range and the other sites here are poleward of it.

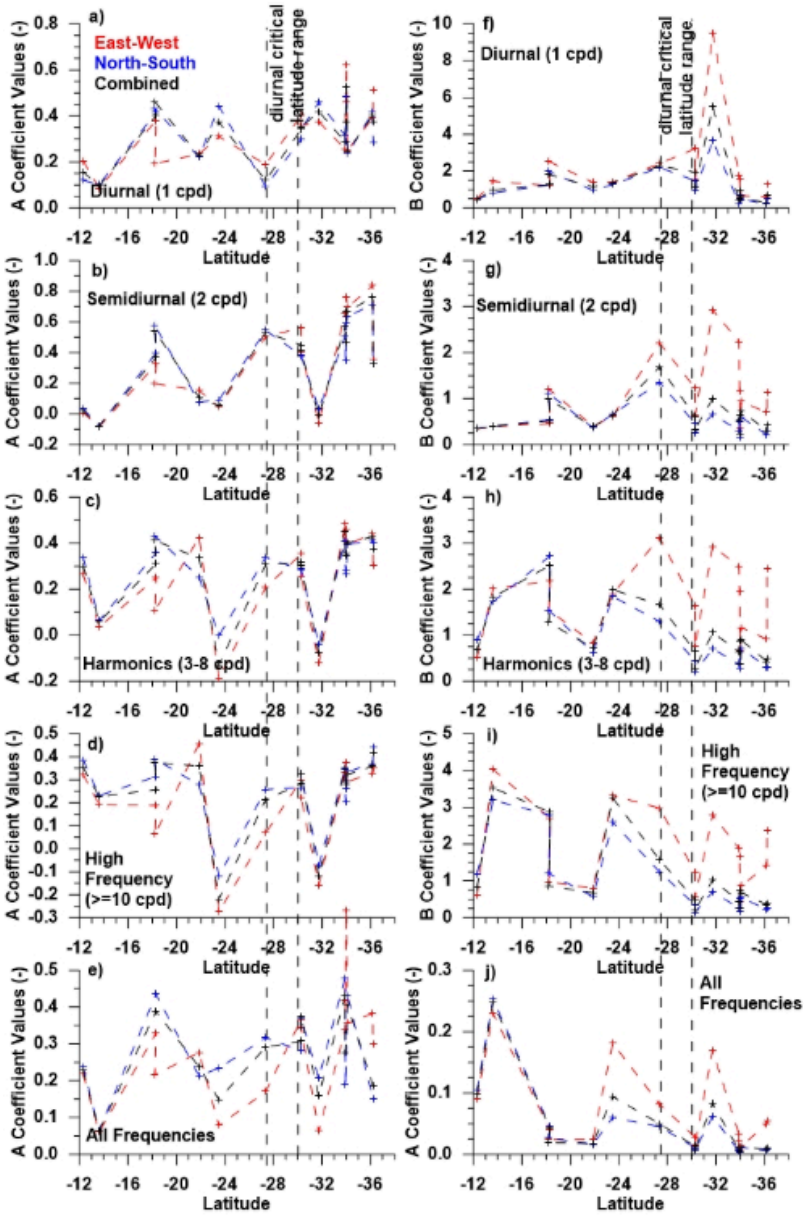

Figure 8

The a-e) A and f-j) B coefficients for the 16 sites based on their latitude with the East-West velocity in red, the North-South velocity in blue, and the combined velocities in black. Five different frequency bands are shown: a & f) diurnal, b & g) semidiurnal, c & h) harmonics (3-10 cpd), d & i) high frequency (>10 cpd), and e & j) all frequencies. The diurnal critical latitudes for O_1 (27.6^{o}S) and K_1 (30°S) are indicated by dashed lines and the diurnal critical latitude range is labeled.

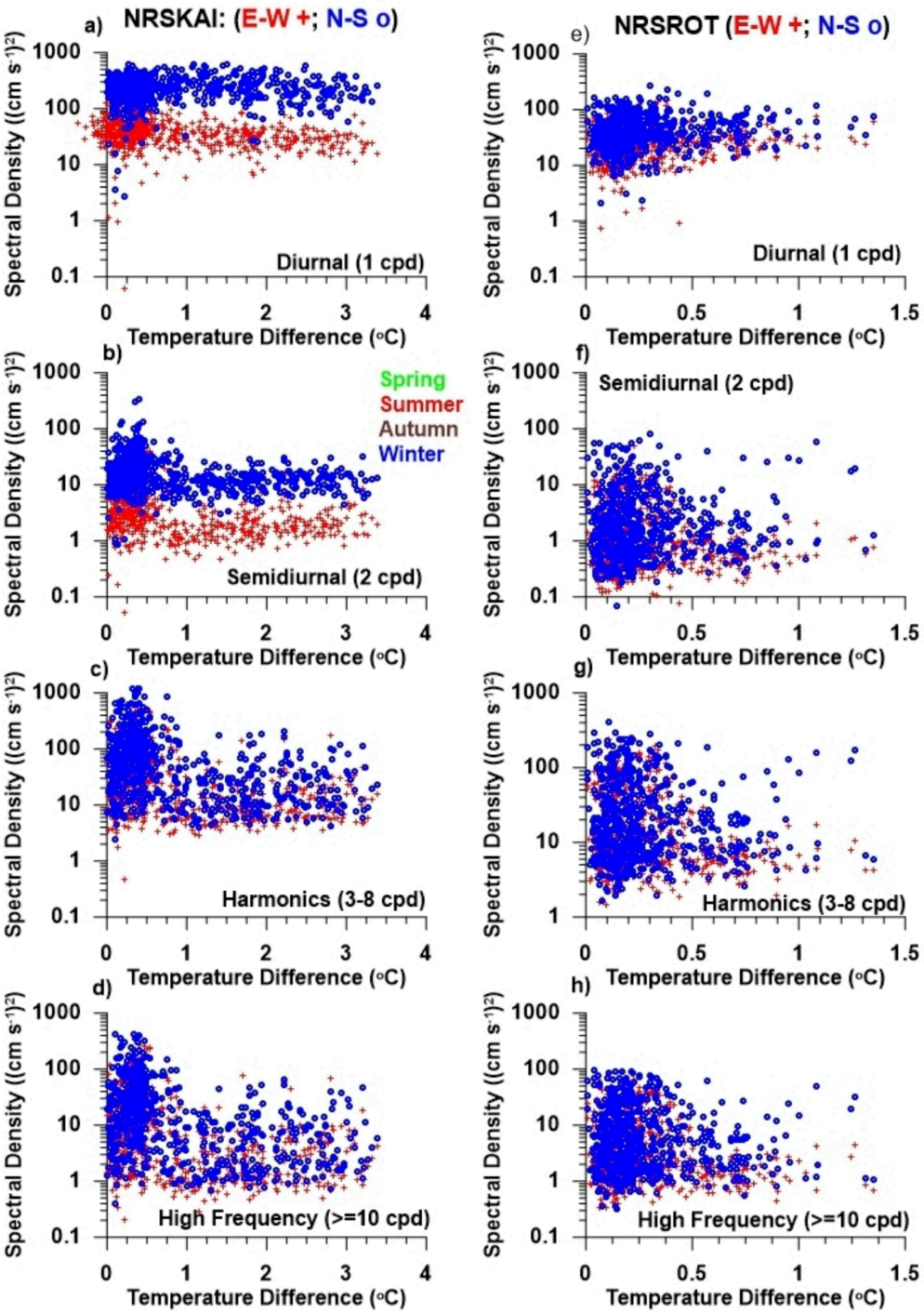

Figure 9

The baroclinic spectral density versus the upper ocean to bottom temperature difference for East-West (red +) and North-South (blue o) velocities from two sites where there was no relationship between the baroclinic spectral density and the upper ocean to bottom temperature differences: a-d) NRSKAI and e-h) NRSROT for four different frequency bands: a & e) diurnal, b & f) harmonics (3-10 cpd), c & g) semidiurnal, and d & h) high frequency (>10 cpd).

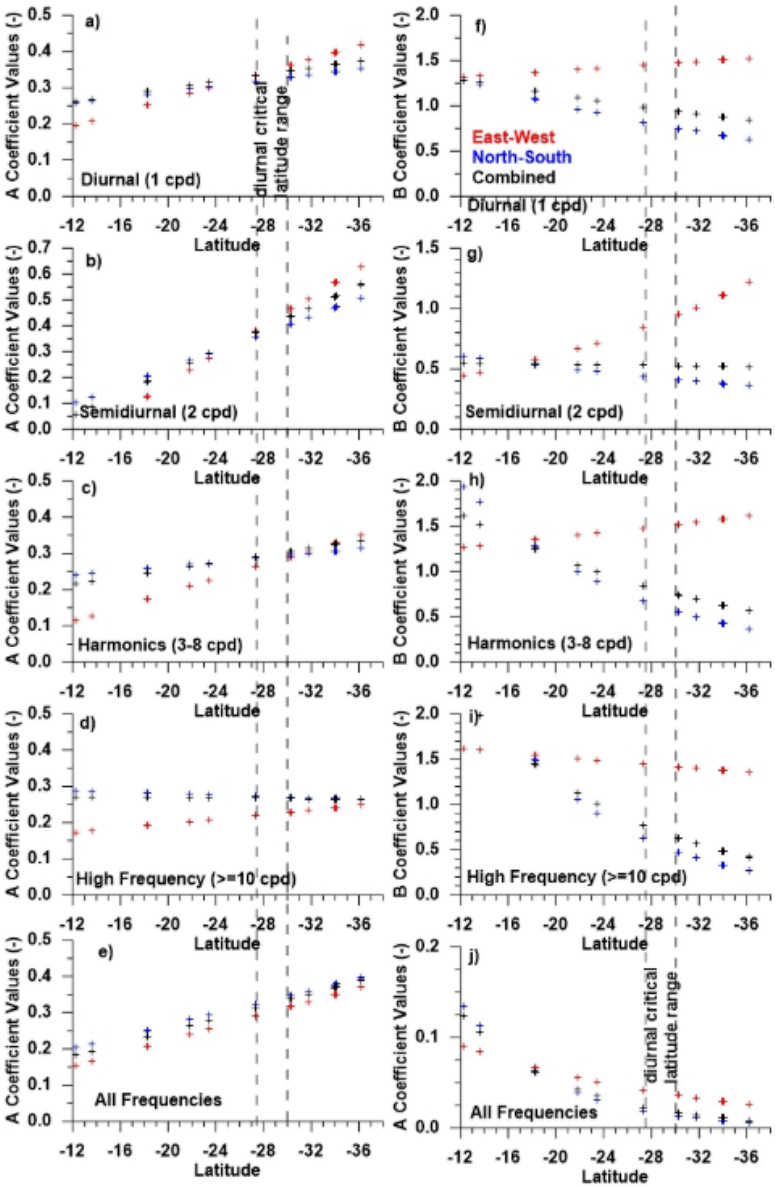

Figure 10

The latitude dependent coefficients for a-e) A and f-j) B for the 16 sites based on their latitude with those for the East-West velocity in red, the North-South velocity in blue, and the combined velocities in black. Five different frequency bands are shown: a & f) diurnal, b & g) semidiurnal, c & h) harmonics (3-10 cpd), d & i) high frequency (>10 cpd), and e & j) all frequencies. The diurnal critical latitudes for O_1 (27.6^{o}S) and K_1 (30°S) are indicated by dashed lines and the diurnal critical latitude range is labeled.

Supplementary Files

This is a list of supplementary files associated with this preprint. Click to download.

- TdiffvsIWERelationSupportingInfoGL.docx